ACS Catalysis

pubs.acs.org/acscatalysis Research Article

Electrolyte Organization Leads to Potential-Dependence in Thermochemical Catalysis of Nonpolar Reactions

Thejas S. Wesley, Yuriy Román-Leshkov,* and Yogesh Surendranath*

Cite This: https://doi.org/10.1021/acscatal.5c09158 Read Online

ACCESS | Metrics & More | Article Recommendations | Supporting Information

ABSTRACT: Electrochemical polarization is now known to play a key role in thermochemical catalysis at solid−liquid interfaces. However, existing frameworks cannot account for why even nonpolar, nonfaradaic reactions are sensitive to interfacial polarization. In order to uncover the molecular basis of this phenomenon, we herein study the potential-dependent reaction kinetics of ethylene and *trans*-2-butene hydrogenation at Pt−liquid interfaces. Measurements were performed in aqueous and *ortho*-difluorobenzene (*o*-DFB) solutions, spontaneously polarizing the Pt−liquid interfaces by, respectively, varying the pH or dissolving distinct metallocene redox buffers into solution. We find that at comparable mechanistic regimes, the rates of both ethylene and *trans*-2-butene hydrogenation are maximized near the same electrochemical potential, *E*. Moreover, the potential-dependence, defined as $\frac{\partial \ln r}{\partial E}$, of *trans*-2-butene hydrogenation is approximately 2.2× greater than that of ethylene hydrogenation across the full potential range studied. These observations are all consistent with a model in which polarization of the Pt surface away from the local potential of zero free charge (E_{PZFC}) induces electrostatic organization of the polar solvent and charged ions near the interface, which impedes olefin adsorption and surface reaction because these surface reactions induce electrolyte displacement. Accordingly, interfacial polarization alters the free energy landscape and thus the rate of nonpolar heterogeneous catalysis by controlling the degree of electrostatic organization of polar and charged spectators at the interface, which do not in general need to be specifically chemisorbed onto the surface but could simply be close enough to the surface to be perturbed by the olefin adsorption. These results point toward electrochemical design handles, namely, the electrolyte, catalyst potential, and local E_{PZFC} of the catalyst, with which to tune interfacial catalysis of thermochemical organic transformations.

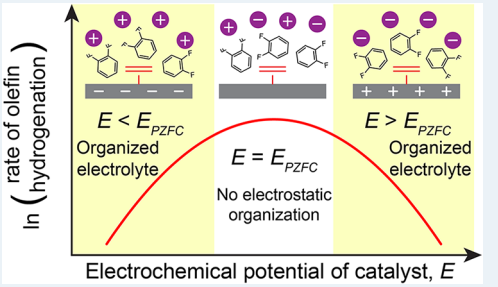

KEYWORDS: *hydrogenation, heterogeneous catalysis, solvent effects, platinum, electric fields, polarization, redox mediators, open-circuit potential*

INTRODUCTION

Electrochemical polarization is known to play an important role in molecular,[1−7] biological,[8,9] and heterogeneous catalysis.[10−18] Such polarization effects are generally expected to arise from the electrostatic profile acting on polar or charged species to alter the free energy landscape of the reaction. However, a generalizable and predictive framework for the mechanistic basis of polarization effects does not yet exist for nonfaradaic transformations of neutral species catalyzed by metal−liquid interfaces, which comprise a broad swath of heterogeneous catalysis. For catalytic metal−liquid interfaces, this knowledge gap stems from multiple complicating factors, including difficulties in measuring the catalyst potential at the distributed interfaces typically used in heterogeneous catalysis,[16,19,20] as well as challenges in determining the interfacial structure of polarized solid−liquid interfaces. Yet, a molecular-level understanding of how interfacial polarization impacts heterogeneous catalysis would enable the practical use of electrochemical design handles to tune thermochemical reaction processes.

In order to determine the role of polarization in nonfaradaic metal-catalyzed reactions, we previously investigated the polarization-dependence of ethylene hydrogenation at Pt−liquid interfaces as one of the simplest probe reactions of this class. We observed that spontaneous interfacial polarization plays a defining role in controlling the rate of liquid-phase ethylene hydrogenation across aqueous and polar aprotic solutions alike.[16] However, given that the reaction comprises nonfaradaic elementary steps involving only uncharged, negligibly polar species, the physical basis and mechanistic origin of the potential-dependence of this probe reaction, and thus the molecular basis for polarization effects in heterogeneous metal catalysis more generally, have remained unclear.

Received: December 21, 2025
Revised: March 6, 2026
Accepted: March 9, 2026

To resolve this conundrum and uncover the origin of these observed electrochemical effects, we herein investigate the potential-dependent reaction kinetics of ethylene and *trans*-2-butene hydrogenation at Pt−liquid interfaces. Measurements were performed in aqueous and *ortho*-difluorobenzene (*o*-DFB) solutions, spontaneously polarizing the Pt−liquid interfaces by, respectively, varying the pH or dissolving distinct metallocene redox buffers into solution. We find that at comparable mechanistic regimes in an *o*-DFB solvent, the rates of both ethylene and *trans*-2-butene hydrogenation are maximized near the same electrochemical potential, E, and that this potential of maximum rate coincides with the potential of zero free charge (E_{PZFC}) for Pt. Moreover, the potential-dependence, defined as $\left(\frac{\partial \ln r}{\partial E}\right)_T$, of *trans*-2-butene hydrogenation is approximately 2.2× greater than that of ethylene hydrogenation across the full potential range studied in *o*-DFB. Finally, ethylene hydrogenation reaction orders remain positive and relatively constant across the full potential range, including on either side of the potential of maximum rate. By extending the long-standing literature on potential-dependent organic adsorption thermodynamics[21−33] to analyze nonfaradaic reaction kinetics, we conclude that our observations are all consistent with a model in which polarization of the Pt surface away from E_{PZFC} induces electrostatic organization of polar or charged spectators (i.e., solvent or electrolyte ions) near the interface, which impedes olefin adsorption and surface reaction because these reactions require electrolyte displacement.

METHODS

Chemicals and Materials

Detailed descriptions of the chemicals used and methods for reagent preparation, purification, and handling are included in the Supporting Information (SI, Section 1.1).

Catalyst Preparation

Pt/C catalysts were prepared via incipient wetness impregnation according to a previously reported method.[16] Vulcan carbon was pretreated for 6 h under flowing H_2 at 1223 K. Subsequently, an aqueous solution of chloroplatinic acid was added dropwise to the high-temperature treated carbon, with careful mixing throughout, until the point of incipient wetness was reached. The resulting material was then dried in air at 403 K for 2 h and then reduced under flowing H_2 at 573 K for 4 h. The catalyst was finally cooled to room temperature and passivated via gradual diffusion of air. Pt loadings were determined via inductively coupled plasma-mass spectrometry. Additional details regarding catalyst preparation are provided in the SI, Section 1.2, including particular considerations regarding handling the reduced-and-passivated catalysts for aqueous and nonaqueous rate measurements, respectively.

Aqueous Ethylene Hydrogenation Studies

Aqueous ethylene hydrogenation experiments were performed in a well-mixed slurry reactor, using a custom, jacketed, gas-tight, five-neck glass cell as previously described.[16] The cell was equipped with a magnetic stir bar, borosilicate sparge tube, a perfluoroalkoxy-coated K-type thermocouple, and a freshly flame-annealed Pt wire, all of which were immersed directly in the fluid contained in the cell. Gas flows (H_2, C_2H_4, He) were controlled using calibrated mass flow controllers and directed into the cell through the sparge tube. During the reaction, the cell pressure was maintained at approximately 1 atm, and the temperature was maintained at 273 K via a circulating chiller.

To begin each reaction, the appropriate quantity of the reduced-and-passivated catalyst was added to the cell, and the cell was purged with flowing He for 5 min to remove air. Then, the catalyst was prereduced with flowing H_2 at room temperature (294 ± 1 K) for at least 90 min, stirring at 300 rpm. Subsequently, a Ag/AgCl reference electrode—specified by the manufacturer to have a zero electrolyte leak rate to prevent chloride contamination of the reaction solution—was installed, followed by the addition of 20 mL of electrolyte. In each experiment, the electrolyte (0.001 M total ionic strength) was freshly prepared using $NaClO_4$ as the supporting electrolyte and adjusting the pH with NaOH or $HClO_4$, maintaining a total ionic strength of 0.001 M. The stirring speed was then increased to 1600 rpm and the cell cooled to 273 ± 1 K. The gas flow was then switched to a mixture of 5 kPa ethylene and 96 kPa H_2 to start the reaction. The reactor effluent was analyzed by using an online gas chromatograph equipped with a flame-ionizing detector and a water-tolerant column. Total carbon balances were always within 5%, which is within the gas chromatograph injection error. Turnover rates are corrected for first-order deactivation by extrapolating measured rates back to zero time-on-stream with a fitted exponential decay (see Figure S1a for a representative protocol), as previously reported.[16] Turnover rates are reported as the rate of ethane formation per surface Pt (see the SI, Section 1.2, for site quantification details). Pt wire open-circuit potentials were monitored throughout the course of the reaction. All ethylene hydrogenation rates were measured at differential (i.e., <2%) conversion, and these protocols enabled rate measurements free from interphase and intraparticle diffusion limitations.[16] Additional details regarding aqueous rate measurements, including all equipment specifications, gas flow rates, catalyst and cell handling, pH measurements, potential referencing, and safety considerations, are listed in the SI, Section 1.3.

Nonaqueous Ethylene Hydrogenation Studies

Nonaqueous ethylene hydrogenation experiments were performed using mostly the same apparatus as the aqueous measurements except that the cell was additionally equipped with a freshly polished glassy carbon rod electrode. Open-circuit potentials of the Pt wire and glassy carbon rod were simultaneously measured throughout the course of the reaction. Nonaqueous electrolytes were prepared using a stock solution of 0.2 M tetrabutylammonium hexafluorophosphate ($TBAPF_6$) in *o*-DFB that was prepared, stored, and handled in a N_2 glovebox. Prior to each reaction, the desired electrolyte was prepared in the N_2 glovebox by adding a 12 mL aliquot of the stock $TBAPF_6$/*o*-DFB solution to a septum-capped glass vial containing appropriate quantities of metallocene (decamethylcobaltocene, cobaltocene, decamethylmanganocene, decamethylferrocene, ferrocene, acetylferrocene, or 1,1′-dibromoferrocene) and the corresponding metallocenium hexafluorophosphate to achieve the desired redox buffer. After equipping the cell with the catalyst and following a 2 h, room-temperature catalyst prereduction under flowing H_2, the Ag/AgCl reference electrode was installed and the cell was then purged with flowing He and H_2 for at least 5 min. Then, with this gas mixture continuing to flow through the cell, the electrolyte (still sealed under N_2) was cannula-transferred to the cell by using He back-pressure. The stirring speed was then increased to 1600 rpm, and the cell was cooled to 273 ± 1 K. The gas flow was finally switched to a mixture of 5 kPa ethylene and 96 kPa H_2 to start the reaction. Similarly to the aqueous rate measurements, rates were corrected for first-order deactivation (Figure S1a). All nonaqueous ethylene hydrogenation rates were measured at <13% ethylene conversion. Additional details regarding nonaqueous ethylene hydrogenation rate measurements, including all reagent preparation and handling, redox buffer preparation, equipment specifications, catalyst and cell handling, potential referencing, and safety considerations, are included in the SI, Section 1.4.

Nonaqueous *trans*-2-Butene Hydrogenation Studies

Nonaqueous *trans*-2-butene hydrogenation experiments were performed essentially identically to the nonaqueous ethylene hydrogenation experiments, using a standard inlet gas composition of 0.07 kPa *trans*-2-butene, 101 kPa H_2, and 0.3 kPa He. Rates were either stable over time (in which case rates are reported as time averages once pseudosteady-state operations were reached, see Figure S1b) or were corrected for slow first-order deactivation (see Figure S1c). We

https://doi.org/10.1021/acscatal.5c09158
ACS Catal. XXXX, XXX, XXX−XXX

note that due to the higher solubility of *trans*-2-butene in *o*-DFB than ethylene, and the low *trans*-2-butene molar flow rate, hydrodynamic transients of slightly more than 1 h were observed upon initiating the reaction. This precluded using decamethylcobaltocene and 1,1′-dibromoferrocene redox buffers, which do not stably pin for sufficiently long as to obtain pseudosteady-state rate measurements. Additional details regarding nonaqueous *trans*-2-butene hydrogenation rate measurements, including considerations regarding *trans*-2-butene quantification and conversion, gas flow rates, and catalyst and cell handling, are included in the SI, Section 1.5.

RESULTS AND DISCUSSION

To elucidate the origin of the potential-dependence of nonpolar hydrogenation catalysis, and thus uncover more generalizable principles governing polarization effects in heterogeneous catalysis, we examined the impact of ionic strength on the polarization-dependence of aqueous ethylene hydrogenation over Pt/C. The Gouy−Chapman−Stern (GCS) model of the electrochemical interface[21,22] predicts that lowering the ionic strength increases the length of the diffuse double-layer and decreases the concentration of ions at the inner Helmholtz (or reaction) plane, thereby reducing the magnitude of the interfacial electric field at a given potential. By systematically varying the ionic strength, we can modulate the magnitude of the interfacial electric field at a given catalyst electrochemical potential, *E*. Accordingly, we hypothesized that measuring aqueous ethylene hydrogenation rates as a function of *E* and ionic strength and comparing these rates to the gas-phase value would provide mechanistic insight into the molecular origins of the observed effects of interfacial charge separation.

Following prior methods, experiments were performed using a well-mixed slurry reactor, with a Pt wire sensing electrode and a Ag/AgCl reference electrode providing an operando measurement of the Pt open-circuit potential (E_{OCP}).[16] Reactions were performed at 273 K by sparging the gaseous olefin and hydrogen through a liquid electrolyte containing suspended Pt/C particles. The catalyst potential, E_{OCP}, was controlled by simply altering the pH, relying on spontaneous proton transfer to polarize the interface.[14,16] We have previously shown that the Pt sensing wire contributes negligibly to measured rates and that the measured rates are free from mass transfer artifacts.[16] Thus, our rate measurements reflect the intrinsic catalytic activity of the dispersed Pt/C particles.

Aqueous ethylene hydrogenation rates versus E_{OCP} at two different solution ionic strengths are shown in Figure 1. We previously reported potential-dependent rates in electrolytes with an ionic strength of 0.1 M[16] and observed an exponential dependence of rate on potential, with a log−linear slope of $\left(\frac{\partial \ln r}{\partial E}\right)_T = 1.9\ V^{-1}$ (data reproduced[16] in Figure 1, dark blue circles). Upon reducing the ionic strength to 0.001 M, the potential-dependence is reduced to a log−linear slope of $\left(\frac{\partial \ln r}{\partial E}\right)_T = 1.1\ V^{-1}$ (Figure 1, light blue circles). The plots of rate vs E_{OCP} across the two ionic strengths generally tend, within experimental error, to converge as E_{OCP} approaches the potential of zero free charge inferred for Pt under aqueous olefin hydrogenation conditions at room temperature ($E_{PZFC} \approx -0.06$ V vs standard hydrogen potential (SHE)).[14] Furthermore, the rate at which the two plots converge near E_{PZFC} is approximately equal to the gas-phase rate, 3.0 s^{-1}, measured at identical partial pressures and temperature.[34] We note that the ratio of the two slopes is similar to the GCS prediction for the ratio in the magnitude of electric fields near the reaction plane for 0.1 vs 0.001 M electrolytes (see the SI, Section 2.1 and Figure S2). Taken together, these observations indicate that near E_{PZFC}, liquid water appears to negligibly impact the observed rate relative to the gas-phase. Moreover, increasing the magnitude of negative interfacial electric fields, through either negative polarization or higher ionic strength at a given potential, attenuates the rate of aqueous ethylene hydrogenation.

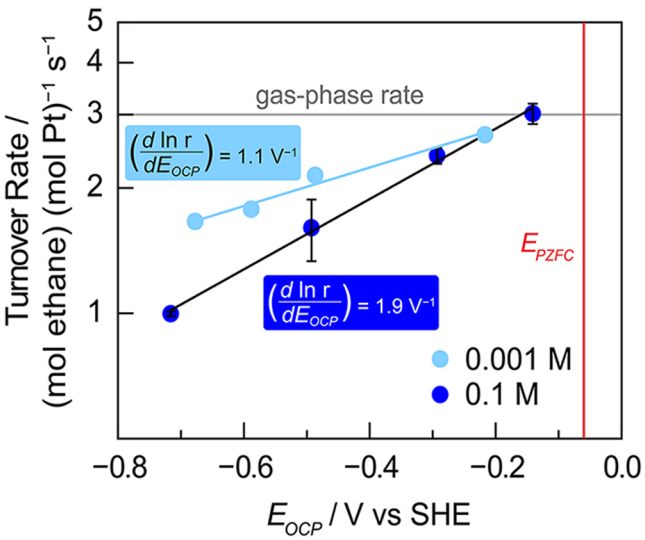

Figure 1. Comparison of the E_{OCP}-dependence of aqueous ethylene hydrogenation rates across two different ionic strengths. 0.1 M data (dark blue) are reproduced from ref 16. (Available under a CC-BY-NC-ND 4.0 license. Copyright 2021 Wesley, T. S.; Román-Leshkov, Y.; Surendranath, Y.) Condition: 273 K, 5 kPa ethylene, 96 kPa H_2, 0.001 or 0.1 M $NaClO_{4(aq)}$, 0.2 wt % Pt/C, E_{OCP} varied by adjusting pH, pH adjusted by addition of $HClO_4$, NaOH, or borate buffer. The gray horizontal line indicates the gas-phase ethylene hydrogenation rate reported for identical partial pressures and temperature.[34] The red vertical line denotes the value reported for the potential of zero free charge for Pt nanoparticles under aqueous hydrogenation conditions.[14]

These observations regarding the impact of negative polarization naturally raise the question of how polarizing the Pt catalyst positive of E_{PZFC} would impact the rate. However, performing such measurements in aqueous electrolytes is challenging because under hydrogenation conditions the Pt E_{PZFC} is near the standard hydrogen potential (SHE). This makes it infeasible to spontaneously polarize Pt significantly positive of E_{PZFC} because even reducing the pH to 0 (standard hydrogen condition) would not lead to polarization positive of E_{PZFC}. While one could easily use a potentiostat to polarize a Pt/C electrode anodically of E_{PZFC} by passing faradaic current (or by using an oxidizing redox buffer), such driven polarization would likely introduce convolutions from mass transfer limitations (i.e., gradients in local H_2 activity or pH) due to parasitic electrochemical hydrogen oxidation. To avoid these complications, we performed ethylene hydrogenation in *o*-DFB, a polar aprotic solvent that permits spontaneous polarization to significantly more positive potentials. Indeed, the lack of any significant proton acceptor in *o*-DFB shifts the thermodynamic potential for hydrogen oxidation much more positive, and thus shifts the

https://doi.org/10.1021/acscatal.5c09158
ACS Catal. XXXX, XXX, XXX−XXX

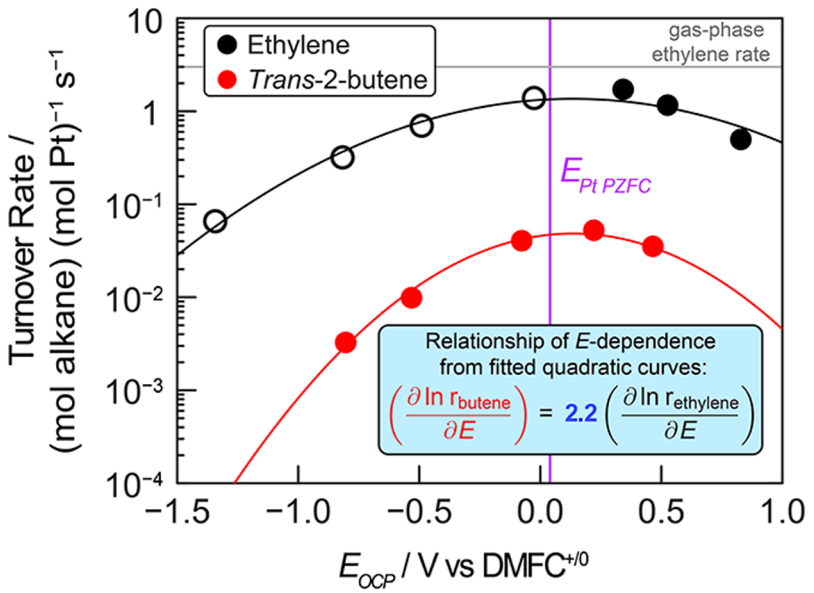

Figure 2. E_{OCP}-dependence of ethylene and *trans*-2-butene hydrogenation rates in *ortho*-difluorobenzene (*o*-DFB) electrolytes on a Pt/C catalyst. Data in open black circles are reproduced from ref 16. (Available under a CC-BY-NC-ND 4.0 license. Copyright 2021 Wesley, T. S.; Román-Leshkov, Y.; Surendranath, Y.) Metallocene-based outer-sphere electron transfer reactions are used to spontaneously polarize Pt via outer-sphere electron transfer during and in parallel to olefin hydrogenation catalysis. The gray horizontal line indicates the gas-phase ethylene hydrogenation rate reported for identical partial pressures and temperature.[34] The purple vertical line denotes the value reported for the potential of zero free charge for polycrystalline Pt in acetonitrile.[35,36] Conditions: 5 kPa ethylene or 0.05 kPa *trans*-2-butene, 96 kPa H_2, 273 K, 0.2 M tetrabutylammonium hexafluorophosphate in *o*-DFB, 0.24 wt % Pt/C.

effective reversible hydrogen potential far more positive relative to E_{PZFC} than in water.

In our previous study,[16] we demonstrated that metallocene redox buffers—namely, decamethylcobaltocene (DMCc), cobaltocene (Cc), decamethylmanganocene (DMMc), and decamethylferrocene (DMFc)—are effective for spontaneously polarizing Pt-*o*-DFB interfaces via outer-sphere electron transfer (OSET) during ethylene hydrogenation catalysis. In this study, we were able to expand the anodic limit of our potential range more positively by employing three additional metallocene redox buffers: ferrocene (Fc), 1,1′-dibromoferrocene (DBFc), and acetylferrocene (AcFc). This set of seven metallocene redox buffers provided access to a potential range of over 2 V over which to study olefin hydrogenation kinetics in *o*-DFB.

Ethylene hydrogenation rates in *o*-DFB are reported in Figure 2 over a 2.17 V range in E_{OCP}, established by spontaneous polarization via the OSET between the Pt/C surface and each of the seven distinct metallocene redox buffers. As previously reported,[16] in the presence of a DMFc (Pt E_{OCP} = −0.03 V vs $DMFc^{+/0}$), DMMc (Pt E_{OCP} = −0.49 V vs $DMFc^{+/0}$), Cc (Pt E_{OCP} = −0.82 V vs $DMFc^{+/0}$), or DMCc (Pt E_{OCP} = −1.34 V vs $DMFc^{+/0}$) redox buffer, rates systematically decreased with increasingly negative potentials, with turnover rates of 1.4 ± 0.2, 0.7 ± 0.04, 0.32 ± 0.02, and 0.066 ± 0.01 s^{-1}, respectively (Figure 2, unfilled black circles, reproduced from prior study[16]). Upon expanding the potential range more positive of −0.03 V vs $DMFc^{+/0}$ using more oxidizing metallocene buffers, we measured a rate of 1.7 s^{-1} in the presence of AcFc at a pseudosteady-state potential of E_{OCP} = +0.34 V vs $DMFc^{+/0}$ (Figure 2, filled black circle). We note that this potential is considerably negative of the thermodynamic potential for AcFc in *o*-DFB. We ascribe this discrepancy to the AcFc buffer (possibly due to the carbonyl moiety) shifting the reversible hydrogen potential sufficiently negative so as to induce a mixed contribution between H^+/H_2 interconversion and the contribution of the OSET to the AcFc buffer in establishing E_{OCP}. This highest observed rate is followed by a decrease in rate in the presence of Fc (E_{OCP} = +0.53 V vs $DMFc^{+/0}$) and DBFc (E_{OCP} = +0.83 V vs $DMFc^{+/0}$), with turnover rates of 1.2 and 0.50 s^{-1}, respectively (Figure 2, filled black circles). As previously noted, the gas-phase rate under similar conditions (5 kPa ethylene, 96 kPa hydrogen, 273 K) has been previously reported to be 3.0 s^{-1}.[34] Thus, the dependence of ethylene hydrogenation rate on potential is nonmonotonic, exhibiting a rate maximum that approaches the gas-phase rate under similar conditions.

While a measurement of E_{PZFC} in *o*-DFB has not been reported to our knowledge, and measuring this value in *o*-DFB proved intractable in our hands (see the SI, Section 2.3, for further discussion), a value of −0.48 V vs Ag/0.1 M $AgNO_3$ has been reported for polycrystalline Pt in acetonitrile.[35] Using a previously reported measurement of $Fc^{+/0}$ and Ag/1 M $AgNO_3$ in acetonitrile vs a common reference electrode,[36] the E_{PZFC} of polycrystalline Pt in acetonitrile on our potential scale is +0.04 V vs $DMFC^{+/0}$ (Figure 2). Importantly, this E_{PZFC} value approximately coincides with the potential region where the ethylene hydrogenation rate is maximized (Figure 2, see below for a detailed discussion).

We have previously shown that metallocene adsorption is unlikely to cause rate attenuation,[16] suggesting that the decrease in rate with Fc and DBFc buffers does not arise from that effect. We next considered whether the interfacial polarization shifts the isotherm for ethylene or hydrogen adsorption to a site-blocking regime. This scenario would require a negative reaction order in either ethylene or hydrogen over a certain potential range. To test this hypothesis, we measured ethylene and hydrogen reaction orders in *o*-DFB across different potentials.

https://doi.org/10.1021/acscatal.5c09158
ACS Catal. XXXX, XXX, XXX−XXX

The dependence of the ethylene hydrogenation rate on ethylene and hydrogen partial pressure was determined at different potentials. Rates were measured across a range of ethylene (1−5 kPa) and hydrogen (20−96 kPa) partial pressures, holding the other partial pressure constant, using He to make up the balance. Ethylene and hydrogen reaction orders were measured in distinct solutions containing either Cc, DMFc, or Fc redox buffers to spontaneously polarize the Pt−liquid interface to different E_{OCP} values. This selection of redox buffers allowed measuring the reaction orders near and on either side of the potential of maximum rate. For the measurements near the potential of maximum rate, DMFc was chosen rather than AcFc because the DMFc buffer stably pins E_{OCP} over a sufficiently long time to accommodate the measurement of pseudosteady-state rates at each partial pressure condition. In this manner, the potential-dependence of ethylene and hydrogen reaction orders could be measured at potentials near, positive, and negative of the potential of the maximum rate.

Plots of the logarithm of rate versus the logarithm of the ethylene and hydrogen partial pressures are shown in Figure 3a and 3b, respectively. Reaction orders were obtained from the slopes of the resulting linear plots. The ethylene reaction order is 0.5 at E_{OCP} = −0.05 V vs $DMFc^{+/0}$ (DMFc pinning), 0.6 at E_{OCP} = −0.81 V vs $DMFc^{+/0}$ (Cc pinning), and 0.6 at E_{OCP} = +0.46 V vs $DMFc^{+/0}$ (Fc pinning), showing a modest, if any, potential-dependence. The hydrogen reaction order is 0.3 at E_{OCP} = −0.08 V vs $DMFc^{+/0}$ (DMFc pinning) and 0.1 at E_{OCP} = −0.79 V vs $DMFc^{+/0}$ (Cc pinning). We also measured ethylene and hydrogen reaction orders in aqueous electrolyte containing 0.1 M $NaClO_4$ (E_{OCP} = −0.28 V vs SHE), pH 5, obtaining a value of 0.6 for ethylene and 0.5 for hydrogen (Figure S3), indicating that our aqueous and nonaqueous ethylene hydrogenation rates reflect a similar mechanistic regime. (See the SI, Section 2.2, for special considerations required for deconvoluting electrochemical from chemical H_2 reaction orders in aqueous solutions.) For comparison, under comparable gas-phase conditions at 273 K, the reaction orders are −0.17 for ethylene (at 20 kPa constant H_2 partial pressure) and 0.67 for H_2 (at both 3.3 and 10 kPa constant ethylene partial pressure).[34]

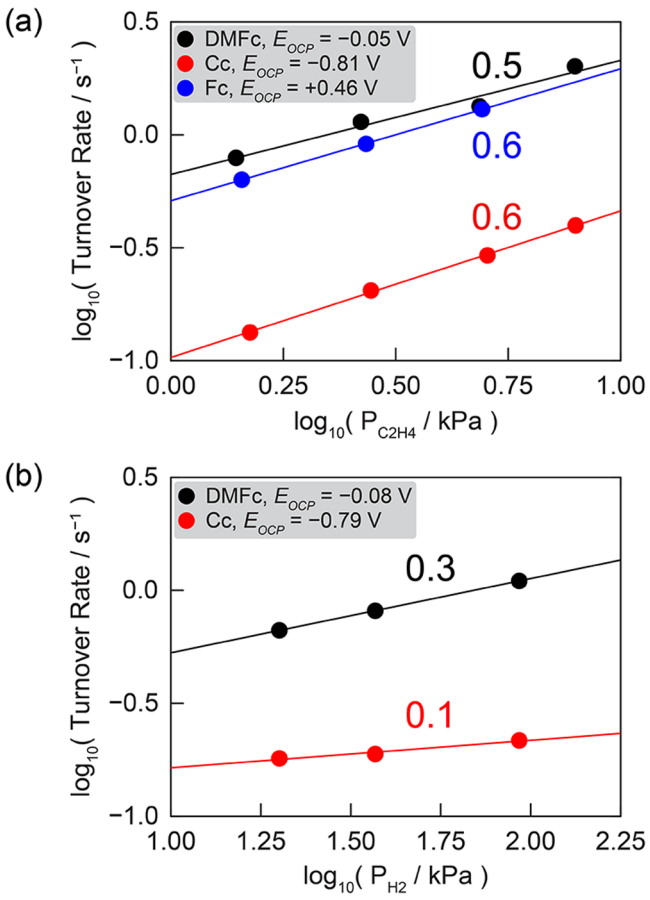

Figure 3. (a) Dependence of ethylene hydrogenation rates on ethylene partial pressures, at different potentials and a constant H_2 partial pressure of 93 kPa. (b) Dependence of ethylene hydrogenation rates on H_2 partial pressures at different potentials and a constant ethylene partial pressure of 5 kPa. Metallocene-based outer-sphere electron transfer reactions are used to spontaneously polarize Pt via outer-sphere electron transfer during and in parallel to olefin hydrogenation catalysis. E_{OCP} values are reported vs $DMFC^{+/0}$. Conditions: 273 K, 0.2 M tetrabutylammonium hexafluorophosphate in *o*-DFB, 0.2 wt % Pt/C.

The fact that reaction orders for both ethylene and hydrogen remain positive across the potential of maximum rate excludes the possibility that the rate inversion across that potential is due to shifting the isotherm of either adsorbate into a high-coverage, site-blocking regime characterized by a negative reaction order. Moreover, the fact that our observed ethylene reaction orders are positive, whereas the comparable gas-phase ethylene reaction order is negative, suggests that the solvent may be abundant on the surface under liquid-phase conditions, inhibiting high olefin coverage.

To rationalize the potential-dependent olefin hydrogenation rates observed in aqueous and nonaqueous solvents, we turned to the long-standing literature on the electrosorption of neutral organic molecules at electrode−solution interfaces.[21−33] In general, it has been observed that the coverage of neutral organic adsorbates exhibits a bell-shaped dependence on electrode potential, with a maximum near the potential of zero free charge (E_{PZFC}).[21] This behavior has been attributed to competitive adsorption between the substrate and the more polar solvent and/or electrolyte ions, since adsorption of any solute must displace adsorbed solvent.[21,26,29,31,32,37−41] Near E_{PZFC}, there are negligible electrostatic interactions between the uncharged surface and solution constituents, lowering the affinity of the polar solvent or ions for the surface and thereby maximizing adsorption of the less polar reactant. In contrast, charging the electrode either negatively or positively of E_{PZFC} introduces electrostatic interactions that drive greater adsorption (both specific and nonspecific) of the more polar or charged constituents in the medium, which in turn inhibits adsorption of the less polar species. Building on this framework, many equations of state have been developed[31] to parametrize the particular quadratic dependence of adsorption free energy on potential in terms of macroscopic physical quantities (e.g., adsorption-induced changes differential capacitance and E_{PZFC}) or molecular properties (e.g., dipole moments, polarizabilities, intermolecular interactions).[21,25,26,29,31−33] These details notwithstanding, the general concept revealed by these thermodynamic studies is that the potential-dependence of neutral organic adsorption at electrode−solution interfaces can largely be explained in terms of a potential-dependent adsorption competition between the adsorbate and polar/charged spectators in solution. However, despite this rich literature on organic electrosorption, these

https://doi.org/10.1021/acscatal.5c09158
ACS Catal. XXXX, XXX, XXX−XXX

results have not yet been connected to the analysis of reaction rates in nonfaradaic catalysis.

Informed by this understanding of potential-dependent adsorption thermodynamics, we hypothesized that the potential-dependence of olefin hydrogenation rate also stems from spontaneous polarization-driven competitive adsorption between the olefin and the solvent or electrolyte ions. In this model, the maximum in olefin hydrogenation rate would be interpreted to approximately reflect the local E_{PZFC} of the catalytic site during catalysis with steady-state coverages of olefin- and H-derived surface intermediates. At this potential, the catalyst sites would be most available for the adsorption and turnover of kinetically competent surface intermediates. Spontaneous polarization negatively or positively of E_{PZFC} induces electrostatic organization of the solvent and/or electrolyte ions near the interface, impeding olefin and H_2 chemisorption and reducing the availability of catalytic sites.

In order to test this polarization-dependent spectator displacement model, we measured the potential-dependence of *trans*-2-butene hydrogenation in *o*-DFB in the presence of different metallocene redox buffers. These measurements were designed to test two predictions of the hypothesized model. First, the model would predict a qualitatively similar nonmonotonic potential-dependence for *trans*-2-butene hydrogenation with a rate maximum at the same potential as that for ethylene hydrogenation. Second, it would also predict a larger potential-dependence for *trans*-2-butene hydrogenation than ethylene hydrogenation since the butene must displace more spectators upon adsorption. Therefore, we aimed to compare the potential-dependence of ethylene to *trans*-2-butene hydrogenation.

trans-2-Butene hydrogenation rate measurements were performed at the same temperature as ethylene hydrogenation (273 K). Partial pressures of *trans*-2-butene and hydrogen were chosen to afford reaction orders that were comparable to those of ethylene hydrogenation in the presence of a DMFc redox buffer. Indeed, to make a fair comparison of potential-dependence across the two reactions, it is necessary to make the comparison at similar mechanistic regimes (i.e., similar surface coverages and reaction orders) rather than at identical partial pressures. With spontaneous polarization set by DMFc pinning, we measured a *trans*-2-butene reaction order of 0.3 in the range of 0.01−0.05 kPa of *trans*-2-butene partial pressure (Figure S4), slightly lower than the 0.5 value measured for ethylene at the same potential. Extending the *trans*-2-butene partial pressure range to lower values was infeasible due to gas chromatograph detection limits and the difficulty of accurately weighing sufficiently small amounts of catalyst to avoid high olefin conversion. Balancing all of these factors, we selected partial pressures of 0.05 kPa *trans*-2-butene and 95 kPa H_2 to measure the potential-dependence of *trans*-2-butene hydrogenation rates across different metallocene redox buffers.

trans-2-Butene hydrogenation rates vs potential are reported in Figure 2 (filled red circles). With a DMFc redox buffer (steady-state Pt E_{OCP} = −0.08 V vs $DMFc^{+/0}$), a rate of 0.041 s^{-1} was observed. With more negative spontaneous polarization, we observe rates of 0.0099 and 0.0033 s^{-1} in the presence of DMMc (Pt E_{OCP} = −0.53 V vs $DMFc^{+/0}$) and Cc (Pt E_{OCP} = −0.80 V vs $DMFc^{+/0}$) redox buffers, respectively. With more positive spontaneous polarization, we observed rates of 0.052 and 0.035 s^{-1} in the presence of AcFc (Pt E_{OCP} = +0.22 V vs $DMFc^{+/0}$) and Fc (Pt E_{OCP} = +0.46 V vs $DMFc^{+/0}$), respectively. We could not measure a steady-state rate in the presence of DBFc (see the SI, Section 1.5 for further explanation). Nevertheless, similarly to ethylene hydrogenation, we observed a nonmonotonic trend with the highest olefin hydrogenation rate obtained with AcFc pinning.

Our measurements permit a quantitative comparison of the potential-dependence of the two olefin hydrogenation reactions. Motivated by the aforementioned quadratic dependence of adsorption free energy on E,[25] we respectively fit the logarithm of ethylene and *trans*-2-butene hydrogenation rates to quadratic functions of E. Given the similar surface chemistries of the two reactions, we would anticipate the Pt E_{PZFC} during reaction to be similar in both cases and thus constrained the model to have the same potential of maximum rate for both quadratics:

$$\ln r_{ethylene} = AE^2 + BE + C$$
$$\ln r_{butene} = \lambda(AE^2 + BE) + D \quad (1)$$

For qualitative interpretation of the significance of parameters A and B, we may turn to quantitative models of the potential-dependence of organic adsorption free energy developed by Frumkin and Butler.[25,26] (See the SI, Section 2.4, for a further description of these models as well as relevant developments in density functional theory.) In Frumkin's adsorption model, based on macroscopic dielectric concepts of capacitance and E_{PZFC}, the quadratic coefficient reflects the difference in interfacial capacitance at zero and full coverage for the adsorbing species due to adsorption-induced changes in the interfacial dielectric constant or double-layer thickness. The linear coefficient reflects a dipolar energy contribution from a change in the E_{PZFC} value induced by adsorption and solvent displacement. In Butler's adsorption model, based on molecular properties, the quadratic coefficient reflects the difference in polarizability between the solvent and the substrate, and the linear term reflects the difference in the dipole moments of the solvent and the substrate. In the context of eq 1, the coefficients A and B would reflect linear combinations of the quantities from each model for each species, weighted by its corresponding generalized[42] degree of rate control.

These quadratic forms closely approximate the potential-dependent rate data (Figure 2). Consistent with the observations in Figure 2, this choice of parametrization ensures that the fitted potential of maximum rates for ethylene and *trans*-2-butene hydrogenation are identical. From the fitted curves, the common potential of maximum rate is given by $E_{max\ rate} = \frac{-B}{2A}$ = +0.13 V vs $DMFc^{+/0}$. We note that errors in referencing and effects due to adsorption of *o*-DFB rather than acetonitrile, and of the olefin and hydrogen during catalysis, could significantly affect the operando local E_{PZFC} relative to the literature value cited. Nonetheless, the fitted potential of maximum rate is remarkably close to the previously reported value of E_{PZFC} = +0.04 V vs $DMFC^{+/0}$ in a nonaqueous electrolyte (see above).[35,36]

The quadratic fits also allow for a quantitative comparison of the slopes of rate versus potential for ethylene and *trans*-2-butene hydrogenation. The derivatives of the fitted equations are related by

$$\frac{\partial \ln r_{butene}}{\partial E} = \lambda \frac{\partial \ln r_{ethylene}}{\partial E} \quad (2)$$

https://doi.org/10.1021/acscatal.5c09158
ACS Catal. XXXX, XXX, XXX−XXX

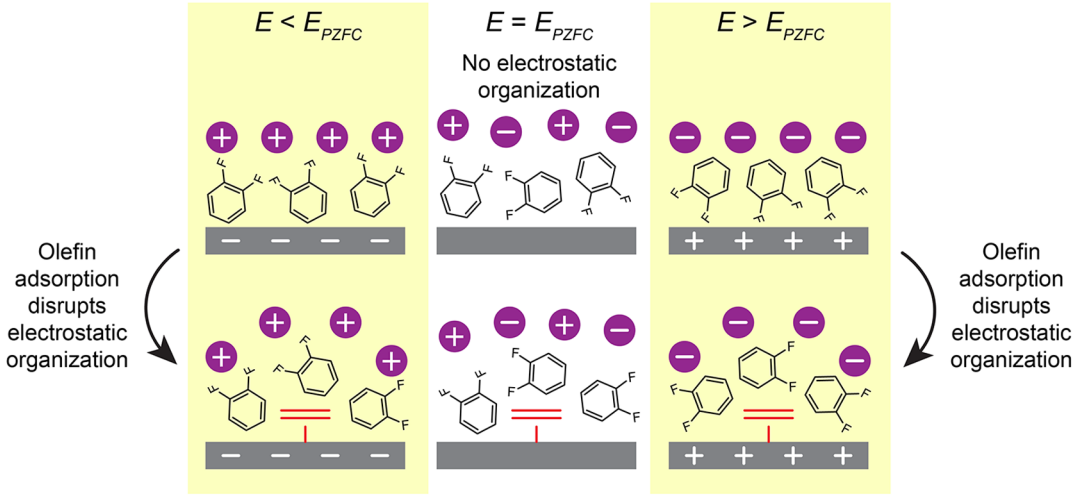

Figure 4. Model of polarization-driven competitive adsorption between the olefin and *o*-DFB and electrolyte ions. Polarization of the catalyst away from the local potential of zero free charge, E_{PZFC}, induces an electrostatic organization of the polar solvent and charged ions within the interphase. This electrostatic organization of spectators alters the free energy landscape and thus rate of reaction by altering the effective number of spectators disrupted or displaced by adsorption and surface reaction of the olefin.

The least-squares regression results in $\lambda = 2.2$, indicating that the rate of *trans*-2-butene hydrogenation is about twice as sensitive to changes in E as that of ethylene hydrogenation across the entire potential range studied. We note that the adsorption "footprint" of *trans*-2-butene on the Pt surface, regardless of whether the adsorbed butene takes the *trans* or *cis* conformation,[43] would be approximately twice that of ethylene. Thus, adsorption of *trans*-2-butene and *trans*-2-butene-drived intermediates would displace approximately twice the amount of solvent or electrolyte ions from the interface as would the adsorption of ethylene and ethylene-derived intermediates. Accordingly, the competitive binding model of polarization-driven solvent/ion adsorption would predict that the rate of *trans*-2-butene hydrogenation would be twice as sensitive to changes in the potential as that of ethylene hydrogenation, precisely as we observe. We further note that the apparent doubling in slope going from ethylene to *trans*-2-butene hydrogenation may suggest that the potential-dependence of this class of olefin hydrogenation reactions, under this regime of operating conditions, arises primarily from properties of the olefin and not the H*.

Finally, we note that the spectator displacement model is also consistent with the observations of aqueous ethylene hydrogenation rates versus potential at different ionic strengths. The plots of rate vs E_{OCP} across the two ionic strengths converge near E_{PZFC} because the interfacial electric field and thus electrolyte organization vanishes near E_{PZFC}, regardless of solution ionic strength. Furthermore, at potentials negative of E_{PZFC}, a lower ionic strength means a smaller electric field and thus less electrostatic organization and competitive binding of the solvent and electrolyte ions; therefore, the slope $\left(\frac{\partial \ln r}{\partial E}\right)_T$ is lower at lower ionic strengths.

Taken together, these results support the assignment of the potential-dependence of olefin hydrogenation to spontaneous polarization-driven competitive adsorption between the olefin and the solvent and/or electrolyte ions (Figure 4). This model resolves the central question of why the rate of nonfaradaic reactions like ethylene or *trans*-2-butene hydrogenation, which involve nonpolar adsorbates with negligible surface dipoles, would depend on interfacial polarization at all. Although the olefins (and H_2) exhibit negligible polarity on the surface, the process of their adsorption and turnover disrupts molecules that are polar and charged within the electrified interphase: the *o*-DFB or water solvent and electrolyte ions.

Importantly, we note that changes in E do not alter whatsoever the electrochemical potential of the interfacial solvent and ions near the interface due to the electrochemical equilibrium established between the interface and the bulk solution. However, polarization of the interface induces an electrostatic organization of the interfacial solvent (in terms of orientation and binding affinity) and electrolyte ions (in terms of concentration and proximity to the interface), which alters the number of those spectators that are disrupted by olefin adsorption and catalysis. We note that these spectators do not, in general, need to be specifically chemisorbed onto the surface but could simply be close enough to the surface or reaction plane to be perturbed by the olefin adsorption. Thus, interfacial polarization alters the free energy landscape and thus the rate of nonpolar heterogeneous catalysis by controlling the degree of electrostatic organization of polar and charged spectators at the interface.

This understanding of the molecular basis for polarization effects in olefin hydrogenation points toward multiple potential design principles for harnessing electrostatics to tune heterogeneous metal catalysis, particularly for organic transformations involving nonpolar or moderately polar substrates. These include the polarity and size of the solvent, the identity and concentration of electrolyte ions, substrate size, steric bulk of particular moieties in multifunctional substrates to tune selectivity, and tuning the local E_{PZFC} of the catalytic site through alloying or support effects. These synthetic handles may be combined with different methods for controlling interfacial polarization at catalytic interfaces: spontaneous polarization via solution redox buffers may be used to polarize distributed catalyst particles in packed-bed or stirred-tank reactors, while driven polarization with wired connections may be applied for catalytic electrodes.

For nonpolar substrates, the main utility of these methods would not be in rate promotion, given that polarization away

https://doi.org/10.1021/acscatal.5c09158
ACS Catal. XXXX, XXX, XXX−XXX

from E_{PZFC} inhibits the rate. Rather, the potential utility for nonpolar substrates could be in mitigating catalyst deactivation or enhancing selectivity between parallel reaction pathways. We may speculate about some possible use cases. For example, the deactivation of Ni-catalyzed, liquid-phase heterogeneous catalysis of cyclohexene hydrogenation is known to proceed via surface hydrocarbon disproportion reactions that have a much higher footprint than the desired hydrogenation pathway;[44] polarization away from E_{PZFC} in such a system might increase catalyst stability. In terms of selectivity, if there are any competing reaction pathways of disparate steric bulk during surface catalysis, then polarization away from E_{PZFC} would be expected to increase the selectivity toward the less bulky surface reactions. Finally, we note that polar substrates would be subject not just to the baseline electrostatic effects of competition with the electrolyte identified herein but might also be susceptible to promotion in absolute reactivity, or it may be possible to reorient the substrate entirely at the interface to alter selectivity.

CONCLUSION

The studies reported here demonstrate that the potential-dependence of olefin hydrogenation catalysis arises from the electrostatic organization of polar solvent or electrolyte ions near the interface. Reaction kinetics measurements for ethylene and *trans*-2-butene hydrogenation were performed on a Pt/C catalyst in *o*-DFB, using metallocene redox buffers to spontaneously polarize the catalytic interface over a greater than 2 V potential span. For both ethylene and *trans*-2-butene hydrogenation, a maximum in the rate is observed near the local E_{PZFC} of Pt. Moreover, the reaction orders in olefin and hydrogen remain relatively constant and positive over the full potential range studied. The rate of *trans*-2-butene hydrogenation is approximately twice as sensitive to changes in E_{OCP} as that of ethylene hydrogenation, consistent with the picture that *trans*-2-butene adsorption would displace roughly twice the amount of electrolyte, as would ethylene adsorption. These observations mirror long-standing adsorption data from electrosorption studies at electrode−solution interfaces, in which the coverage of neutral adsorbates is maximized near E_{PZFC}. Polarizing the catalyst away from this potential introduces electrostatic forces that preferentially drive the adsorption of more polar solvent or electrolyte ions, impeding olefin adsorption and hydrogenation catalysis.

This study establishes that the electrostatic organization of polar and charged spectators, and the motion of these spectators within the electrified interphase upon substrate adsorption and reaction, endows even nonpolar, nonfaradaic reactions with electrochemical handles with which to tune catalysis. More generally, our results highlight the critical importance of considering the structure and motion of solution-phase ions and dipoles in nonfaradaic catalysis at solid−liquid interfaces. Indeed, this work generalizes long-standing concepts of adsorption thermodynamics at solid−liquid interfaces to reaction kinetics. These mechanistic insights suggest that the solvent, electrolyte, catalyst potential, and local E_{PZFC} of the catalyst site, might serve as simple electrochemical design handles with which to tune interfacial catalysis, particularly for organic transformations.

ASSOCIATED CONTENT

Supporting Information

The Supporting Information is available free of charge at https://pubs.acs.org/doi/10.1021/acscatal.5c09158.

Full experimental details and methods; additional reaction order data, as well as estimated electric field ratios in aqueous electrolytes (PDF)

AUTHOR INFORMATION

Corresponding Authors

Yuriy Román-Leshkov − *Department of Chemical Engineering, Massachusetts Institute of Technology, Cambridge, Massachusetts 02139, United States; Department of Chemistry, Massachusetts Institute of Technology, Cambridge, Massachusetts 02139, United States;* orcid.org/0000-0002-0025-4233; Email: yroman@mit.edu

Yogesh Surendranath − *Department of Chemical Engineering, Massachusetts Institute of Technology, Cambridge, Massachusetts 02139, United States; Department of Chemistry, Massachusetts Institute of Technology, Cambridge, Massachusetts 02139, United States;* orcid.org/0000-0003-1016-3420; Email: yogi@mit.edu

Author

Thejas S. Wesley − *Department of Chemical Engineering, Massachusetts Institute of Technology, Cambridge, Massachusetts 02139, United States;* orcid.org/0000-0003-1989-6460

Complete contact information is available at: https://pubs.acs.org/10.1021/acscatal.5c09158

Notes

The authors declare no competing financial interest.

ACKNOWLEDGMENTS

We thank Jaeyune Ryu, John R. Di Iorio, Michael L. Pegis, and Mark M. Sullivan for helpful scientific discussions. We also thank Neil K. Razdan and Karl S. Westendorff for valuable feedback on the manuscript. The electrochemical studies were supported by the Air Force Office of Scientific Research (AFOSR) under Award number FA9550-20-1-0291. The thermochemical studies were supported by the Department of Energy, Office of Basic Energy Sciences, under Award DE-SC0016214. T.S.W. acknowledges support from the National Science Foundation Graduate Research Fellowship under Grant No. 174530.

REFERENCES

(1) Gorin, C. F.; Beh, E. S.; Bui, Q. M.; Dick, G. R.; Kanan, M. W. Interfacial Electric Field Effects on a Carbene Reaction Catalyzed by Rh Porphyrins. *J. Am. Chem. Soc.* **2013**, *135* (30), 11257−11265.

(2) Klinska, M.; Smith, L. M.; Gryn'ova, G.; Banwell, M. G.; Coote, M. L. Experimental Demonstration of pH-Dependent Electrostatic Catalysis of Radical Reactions. *Chem. Sci.* **2015**, *6* (10), 5623−5627.

(3) Azcarate, I.; Costentin, C.; Robert, M.; Savéant, J.-M. Through-Space Charge Interaction Substituent Effects in Molecular Catalysis Leading to the Design of the Most Efficient Catalyst of CO_2-to-CO Electrochemical Conversion. *J. Am. Chem. Soc.* **2016**, *138* (51), 16639−16644.

(4) Reath, A. H.; Ziller, J. W.; Tsay, C.; Ryan, A. J.; Yang, J. Y. Redox Potential and Electronic Structure Effects of Proximal Nonredox

Active Cations in Cobalt Schiff Base Complexes. *Inorg. Chem.* **2017**, *56* (6), 3713−3718.
(5) Chantarojsiri, T.; Ziller, J. W.; Yang, J. Y. Incorporation of Redox-Inactive Cations Promotes Iron Catalyzed Aerobic C-H Oxidation at Mild Potentials. *Chem. Sci.* **2018**, *9* (9), 2567−2574.
(6) Kang, K.; Fuller, J.; Reath, A. H.; Ziller, J. W.; Alexandrova, A. N.; Yang, J. Y. Installation of Internal Electric Fields by Non-Redox Active Cations in Transition Metal Complexes. *Chem. Sci.* **2019**, *10* (43), 10135−10142.
(7) Shaik, S.; Danovich, D.; Joy, J.; Wang, Z.; Stuyver, T. Electric-Field Mediated Chemistry: Uncovering and Exploiting the Potential of (Oriented) Electric Fields to Exert Chemical Catalysis and Reaction Control. *J. Am. Chem. Soc.* **2020**, *142* (29), 12551−12562.
(8) Fried, S. D.; Bagchi, S.; Boxer, S. G. Extreme Electric Fields Power Catalysis in the Active Site of Ketosteroid Isomerase. *Science* **2014**, *346* (6216), 1510−1514.
(9) Liu, C. T.; Layfield, J. P.; Stewart, R. J.; French, J. B.; Hanoian, P.; Asbury, J. B.; Hammes-Schiffer, S.; Benkovic, S. J. Probing the Electrostatics of Active Site Microenvironments along the Catalytic Cycle for *Escherichia Coli* Dihydrofolate Reductase. *J. Am. Chem. Soc.* **2014**, *136* (29), 10349−10360.
(10) Stoukides, M.; Vayenas, C. G. The Effect of Electrochemical Oxygen Pumping on the Rate and Selectivity of Ethylene Oxidation on Polycrystalline Silver. *J. Catal.* **1981**, *70* (1), 137−146.
(11) Vayenas, C. G.; Bebelis, S.; Ladas, S. Dependence of Catalytic Rates on Catalyst Work Function. *Nature* **1990**, *343*, 625−627.
(12) Neophytides, S. G.; Tsiplakides, D.; Stonehart, P.; Jaksic, M. M.; Vayenas, C. G. Electrochemical Enhancement of a Catalytic Reaction in Aqueous Solution. *Nature* **1994**, *370*, 45−47.
(13) Vayenas, C. G.; Bebelis, S.; Pliangos, C.; Brosda, S.; Tsiplakides, D. *Electrochemical Activation of Catalysis: Promotion, Electrochemical Promotion, and Metal-Support Interactions*; Kluwer Academic/Plenum Publishers: New York, 2001.
(14) Ryu, J.; Surendranath, Y. Tracking Electrical Fields at the Pt/H_2O Interface during Hydrogen Catalysis. *J. Am. Chem. Soc.* **2019**, *141* (39), 15524−15531.
(15) Singh, N.; Lee, M.-S.; Akhade, S. A.; Cheng, G.; Camaioni, D. M.; Gutiérrez, O. Y.; Glezakou, V.-A.; Rousseau, R.; Lercher, J. A.; Campbell, C. T. Impact of pH on Aqueous-Phase Phenol Hydrogenation Catalyzed by Carbon-Supported Pt and Rh. *ACS Catal.* **2019**, *9*, 1120−1128.
(16) Wesley, T. S.; Román-Leshkov, Y.; Surendranath, Y. Spontaneous Electric Fields Play a Key Role in Thermochemical Catalysis at Metal−Liquid Interfaces. *ACS Cent. Sci.* **2021**, *7* (6), 1045−1055.
(17) Westendorff, K. S.; Hülsey, M. J.; Wesley, T. S.; Román-Leshkov, Y.; Surendranath, Y. Electrically Driven Proton Transfer Promotes Brønsted Acid Catalysis by Orders of Magnitude. *Science* **2024**, *383*, 757−763.
(18) Dinakar, B.; Westendorff, K. S.; Torres, J. F.; Dakhchoune, M.; Groenhout, K.; Ewell, N.; Surendranath, Y.; Dincă, M.; Román-Leshkov, Y. Elucidating Electric Field-Induced Rate Promotion of Brønsted Acid-Catalyzed Alcohol Dehydration. *J. Am. Chem. Soc.* **2025**, *147* (31), 27599−27610.
(19) Wesley, T. S.; Hülsey, M. J.; Westendorff, K. S.; Lewis, N. B.; Crumlin, E. J.; Román-Leshkov, Y.; Surendranath, Y. Metal Nanoparticles Supported on a Nonconductive Oxide Undergo pH-Dependent Spontaneous Polarization. *Chem. Sci.* **2023**, *14* (26), 7154−7160.
(20) Razdan, N. K.; Westendorff, K. S.; Surendranath, Y. Wireless Potentiometry of Thermochemical Heterogeneous Catalysis. *Nat. Catal.* **2025**, *8* (4), 315−327.
(21) Bockris, J. O.; Reddy, A.; Gamboa-Aldeco, M. *Modern Electrochemistry 2A: Fundamentals of Electrodics*, 2nd ed.; Springer: Boston, MA, 2000.
(22) Schmickler, W.; Santos, E. *Interfacial Electrochemistry*, 2nd ed.; Springer: Heidelberg, 2010.
(23) Frumkin, A. Die Kapillarkurve Der Höheren Fettsäuren Und Die Zustandsgleichung Der Oberflächenschicht. *Z. Phys. Chem.* **1925**, *116U* (1), 466−484.
(24) Frumkin, A. Über Die Beeinflussung Der Adsorption von Neutralmolekülen Durch Ein Elektrisches Feld. *Z. Phys.* **1926**, *35* (10), 792−802.
(25) Frumkin, A. N.; Damaskin, B. B.Adsorption of Organic Compounds at Electrodes. In *Modern Aspects of Electrochemistry*; Butterworths, 1964; Vol. *3*, pp 149−223.
(26) Butler, J. A. V. The Equilibrium of Heterogeneous Systems Including Electrolytes. Part III. The Effect of an Electric Field on the Adsorption of Organic Molecules, and the Interpretation of Electro-Capillary Curves. *Proc. R. Soc. London, Ser. A* **1929**, *122* (790), 399−416.
(27) Gileadi, E.; Rubin, B. T.; Bockris, J. O. M. Electrosorption of Ethylene on Platinum as a Function of Potential, Concentration, and Temperature. *J. Phys. Chem. A* **1965**, *69* (10), 3335−3345.
(28) Barradas, R. G.; Hamilton, P. G.; Conway, B. E. Esin and Markov Effect for Adsorbed Organic Ions and Molecules. *J. Phys. Chem. A* **1965**, *69* (10), 3411−3417.
(29) Bockris, J. O. M.; Gileadi, E.; Müller, K. A Molecular Theory of the Charge Dependence of Competitive Adsorption. *Electrochim. Acta* **1967**, *12* (9), 1301−1321.
(30) Schultze, J. W.; Vetter, K. J. Experimental Determination and Interpretation of the Electrosorption Valency. *J. Electroanal. Chem. Interfacial Electrochem.* **1973**, *44*, 63−81.
(31) Trasatti, S. Acquisition and Analysis of Fundamental Parameters in the Adsorption of Organic Substances at Electrodes. *J. Electroanal. Chem. Interfacial Electrochem.* **1974**, *53*, 335−363.
(32) Koppitz, F. D.; Schultze, J. W.; Rolle, D. The Electrosorption Valency of Organic Electrosorbates: Part I. Aliphatic Compounds. *J. Electroanal. Chem. Interfacial Electrochem.* **1984**, *170*, 5−26.
(33) Rolle, D.; Schultze, J. W. The Electrosorption Valency of Organic Electrosorbates: Part II. Aromatic and Heterocyclic Compounds. *J. Electroanal. Chem. Interfacial Electrochem.* **1987**, *229*, 141−164.
(34) Cortright, R. D.; Goddard, S. A.; Rekoske, J. E.; Dumesic, J. A. Kinetic Study of Ethylene Hydrogenation. *J. Catal.* **1991**, *127* (1), 342−353.
(35) Petrii, O. A.; Khomchenko, I. G. Electrochemical Properties of Platinum and Palladium Electrodes in Acetonitrile Solutions. *J. Electroanal. Chem. Interfacial Electrochem.* **1980**, *106*, 277−286.
(36) Kolthoff, I. M.; Thomas, F. G. Electrode Potentials in Acetonitrile. Estimation of the Liquid Junction Potential between Acetonitrile Solutions and the Aqueous Saturated Calomel Electrode. *J. Phys. Chem. A* **1965**, *69* (9), 3049−3058.
(37) Koppitz, F. D.; Schultze, J. W. Bond Formation in Electrosorbates-II Electrosorption and Double Layer Properties in Non-Aqueous Solvents. *Electrochim. Acta* **1976**, *21* (5), 337−343.
(38) Augustine, R. L.; Techasauvapak, P. Heterogeneous Catalysis in Organic Synthesis. Part 9. Specific Site Solvent Effects in Catalytic Hydrogenations. *J. Mol. Catal.* **1994**, *87* (1), 95−105.
(39) Sievers, C.; Noda, Y.; Qi, L.; Albuquerque, E. M.; Rioux, R. M.; Scott, S. L. Phenomena Affecting Catalytic Reactions at Solid−Liquid Interfaces. *ACS Catal.* **2016**, *6* (12), 8286−8307.
(40) Akinola, J.; Campbell, C. T.; Singh, N. Effects of Solvents on Adsorption Energies: A General Bond-Additivity Model. *J. Phys. Chem. C* **2021**, *125* (44), 24371−24380.
(41) Potts, D. S.; Bregante, D. T.; Adams, J. S.; Torres, C.; Flaherty, D. W. Influence of Solvent Structure and Hydrogen Bonding on Catalysis at Solid-Liquid Interfaces. *Chem. Soc. Rev.* **2021**, *50* (22), 12308−12337.
(42) Stegelmann, C.; Andreasen, A.; Campbell, C. T. Degree of Rate Control: How Much the Energies of Intermediates and Transition States Control Rates. *J. Am. Chem. Soc.* **2009**, *131* (23), 8077−8082.
(43) Zaera, F. The Surface Chemistry of Metal-Based Hydrogenation Catalysis. *ACS Catal.* **2017**, *7*, 4947−4967.

https://doi.org/10.1021/acscatal.5c09158
ACS Catal. XXXX, XXX, XXX−XXX

(44) Boudart, M.; Cheng, W.-C. Catalytic Hydrogenation of Cyclohexene 7. Liquid Phase Reaction on Supported Nickel. *J. Catal.* **1987**, *106*, 134−143.

https://doi.org/10.1021/acscatal.5c09158
ACS Catal. XXXX, XXX, XXX−XXX